Exceptional Points Induced by Time-Varying Mass to Enhance the Sensitivity of Defect Detection

Jinbo Yuan,[1] Linlin Geng,[1] Jiahui Huang,[1] Qiuquan Guo,[2] Jun Yang,[2] Gengkai Hu,[1] and Xiaoming Zhou[1],[*]

[1]*Key Laboratory of Dynamics and Control of Flight Vehicle of Ministry of Education, School of Aerospace Engineering, Beijing Institute of Technology, Beijing 100081, China*

[2]*Shenzhen Institute for Advanced Study, University of Electronic Science and Technology of China, Shenzhen 518110, China*

The exceptional point (EP), a non-Hermitian degeneracy at which eigenvalues and eigenvectors coalesce simultaneously, is investigated in mechanical oscillators involving a time-varying mass. A dynamic modulation mechanism is employed to create the time-varying mass, which can potentially develop an EP by acting as an energy source and drain. To fully demonstrate the existence of EPs, the eigenvalue problem for the modulated system is theoretically formulated through two different schemes, based on the state-space and harmonic balance methods. A second-order EP is confirmed by both methods and exists as a result of the coalescence of fundamental and harmonic eigenmodes. As a salient property of this second-order EP, the square-root behavior of the eigenfrequency subject to small perturbations of the system parameters is theoretically demonstrated, and utilized to devise a proof-of-concept model for mechanical sensors with high sensitivity to void defects in elastic solids. The EP behavior induced by a time-varying mass may find potential applications in damage assessment and health monitoring of engineering structures.

I. INTRODUCTION

Sensor devices that can monitor changes in mechanical environments have a broad range of application in civil, aerospace, and manufacturing engineering. Resonant sensing is a promising sensing method that is based on a shift of the resonant frequency of a vibrating structure subjected to small perturbations that are to be detected. With its features of a high quality factor and the quasidigital nature of the output [1,2], resonant sensing has been widely used in dynamic monitoring [3–5], gas detection [6–8], chemical and biochemical sensing [9–11], etc. Usually, the relationship between the frequency shift and the perturbation is fitted linearly over the dynamic range of the device. This limits the possibilities for improvement of the sensitivity of resonant sensing systems. Great attention has been paid to developing mechanisms for achieving sensitivity enhancement. For example, the variation of the eigenstate amplitude ratio was found to be more sensitive than the shift of the resonant frequency in multidegree-of-freedom resonators [12].

Recently, the exceptional-point (EP) phenomenon in open quantum systems that can exchange energy with their surroundings has provided a different scheme for sensitivity enhancement. An EP is a non-Hermitian degeneracy, at which two or more eigenvalues and their corresponding eigenvectors coalesce simultaneously [13,14]. When the system operates at an nth-order EP, at which n eigenstates are degenerate, a weak perturbation of the system parameters lifts the degeneracy, leading to a frequency splitting proportional to the nth root of the perturbation [15]. Extending this idea to optical and electronic systems, this concept has been used to devise sensing devices with high sensitivity, working especially well for extremely small perturbations. EPs can be created in optical microcavities by tuning the coupling between clockwise- and anticlockwise-traveling modes, and this was demonstrated to be feasible in devices for detecting nanoscale objects [16], measuring rotations (as a sensitive gyroscope) [17], and sensing microstresses with ultrahigh sensitivity [18]. EPs can also be developed in circuit systems and used to design a reconfigurable wireless system for robust and sensitive readout of microsensors [19]. The induction of a sixth-order EP in a circuit system was also demonstrated, which has great application potential in next-generation sensing technologies [20].

The concept of EPs has also been extended to acoustic and mechanical systems. Although eigenstate degeneracy

_____
[*]zhxming@bit.edu.cn

requires only the presence of energy losses [21–28], a rigorous EP with real eigenvalues demands a delicate balance of loss and gain, which is usually obtained by the use of parity-time (*PT*)-symmetric non-Hermitian systems [29,30]. *PT* symmetry was found to be realizable in elastic structures with shunted piezoelectric materials, and the loss-and-gain effect was achieved by introducing positive and negative resistances into shunt circuits [31,32]. Based on this strategy, Wu *et al.* [33] demonstrated an EP in a *PT*-symmetric beam with shunted piezoelectric patches that supported flexural waves. Rosa *et al.* [34] investigated the construction of EPs in continuous elastic media with piezoelectric transducers, and illustrated enhanced sensitivity for sensing point-mass perturbations and crack-type defects. Recently, a different scheme has been proposed using electrical resonators, which develops an EP by temporally periodic variation of circuit parameters in a system without loss and gain elements, but with purely real resonance frequencies [35]. In the present paper, we explore this concept more deeply for mechanical systems.

In the work presented here, we study the EP phenomenon in mechanical resonators coupled to a time-varying mass element. The temporally modulated mass allows an EP to be created in a single resonator without the coupling of multiple resonators, making the EP model more compact and simple. Section II gives a theoretical formulation of the eigenvalue problem for time-varying-mass resonators, which is developed by use of the state-space and harmonic balance methods. In Sec. III, a second-order EP is demonstrated with numerical examples, and the square-root behavior of the eigenvalues with respect to small perturbations is shown. In Sec. IV, we conceive a proof-of-concept model for a mechanical sensor based on the behavior of an EP, and demonstrate its high sensitivity for detecting void defects in elastic materials.

II. FORMULATION OF EIGENVALUE PROBLEM FOR A TIME-MODULATED SYSTEM

A. Model geometry

Consider a mechanical harmonic oscillator consisting of a mass m_0 subjected to a force from a spring with elastic constant K. The eigenfrequency of the oscillator is given simply by $\sqrt{K/m_0}$. Now let us connect the block of mass m_0 to two additional bodies of mass m_1 placed on tracks rotating with an angular frequency ω_r, as schematically depicted in Fig. 1. This model has been demonstrated to produce a time-periodic mass $M(t)$ given by the following expression [36]:

$$M(t) = M_0 \left[1 + \alpha \cos(\omega_m t) \right], \quad (1)$$

where $M_0 = m_0 + m_1$, $\alpha = m_1/M_0$, and $\omega_m = 2\omega_r$. Let $u(t)$ denote the displacement of the mass m_0. The equation
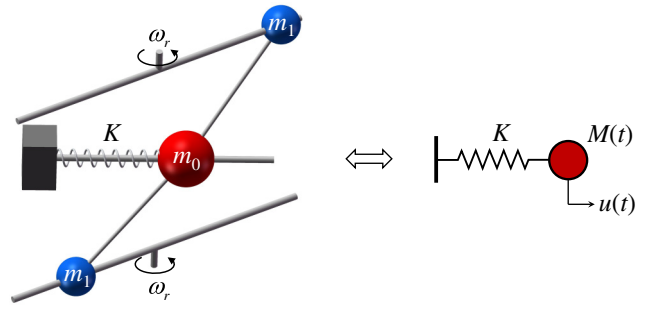

FIG. 1. Mechanical oscillator system consisting of an elastic spring and a time-varying inertial mass.

of motion of the time-varying-mass oscillator is written as

$$\frac{d}{dt}\left[M(t) \frac{d}{dt} u(t) \right] + Ku(t) = 0, \quad (2)$$

or, equivalently,

$$M(t) \frac{d^2 u(t)}{dt^2} + \frac{dM(t)}{dt}\frac{du(t)}{dt} + Ku(t) = 0. \quad (3)$$

The second term in Eq. (3) can be considered as an effective "damping force," where $\zeta(t) = dM(t)/dt$ denotes the damping coefficient, and can be either positive or negative according to Eq. (1). Although the oscillator system does not involve loss and gain elements, $\zeta(t)$ can provide effective loss and gain, which can potentially develop an EP. To demonstrate the existence of EPs, the eigenfrequency of the modulated system needs to be analyzed, which is more complicated than for a harmonic oscillator with a constant mass. In the following sections, we develop a theoretical formulation for solving the eigenvalue problem of Eq. (2) or (3) based on the state-space method and the harmonic balance method, respectively.

B. State-space method

By introducing the state vector $\mathbf{z} = [u, du/dt]^T$, the equation of motion (3) can be written as

$$\frac{d}{dt}\mathbf{z}(t) = \mathbf{R}(t)\mathbf{z}(t), \quad (4)$$

where the 2×2 time-dependent matrix $\mathbf{R}(t)$ is given by

$$\mathbf{R}(t) = \begin{bmatrix} 0 & 1 \\ -K/M(t) & -[dM(t)/dt]/M(t) \end{bmatrix}. \quad (5)$$

The evolution of the state vector $\mathbf{z}$ from the time instant t_0 to t can be expressed as [37]

$$\mathbf{z}(t) = \mathbf{T}(t, t_0)\mathbf{z}(t_0) \quad \text{with } \mathbf{T}(t_0, t_0) = \mathbf{I}, \quad (6)$$

where $\mathbf{T}(t, t_0)$ is referred to as the state transition matrix, and $\mathbf{I}$ is the identity matrix of rank 2 [38]. Using Eq. (6),

the equation of motion (4) can be written in terms of the state transition matrix $\mathbf{T}(t, t_0)$ as

$$\frac{d}{dt}\mathbf{T}(t, t_0) = \mathbf{R}(t)\mathbf{T}(t, t_0). \quad (7)$$

The general expression for the state transition matrix $\mathbf{T}(t, t_0)$ can be expressed as a Peano-Baker series [39,40]

$$\mathbf{T}(t, t_0) = \mathbf{I} + \int_{t_0}^{t} \mathbf{R}(\tau_0)\, d\tau_0 + \int_{t_0}^{t} \mathbf{R}(\tau_0) \int_{t_0}^{\tau_0} \mathbf{R}(\tau_1)\, d\tau_1\, d\tau_0$$

$$+ \int_{t_0}^{t} \mathbf{R}(\tau_0) \int_{t_0}^{\tau_0} \mathbf{R}(\tau_1) \int_{t_0}^{\tau_1} \mathbf{R}(\tau_2)\, d\tau_2\, d\tau_1\, d\tau_0$$

$$+ \cdots \quad (8)$$

Now let us focus on the state evolution within the modulation period $T_m = 2\pi/\omega_m$ of $M(t)$. According to Eq. (6), the state evolution over the time interval $(t, t + T_m)$ can be expressed as

$$\mathbf{z}(t + T_m) = \mathbf{T}(t + T_m, t)\mathbf{z}(t). \quad (9)$$

To calculate $\mathbf{T}(t + T_m, t)$, we divide the time period from t to $t + T_m$ evenly into N portions, with $\delta = T_m/N$ for each one. The temporal evolution of the state vector $\mathbf{z}$ over the period δ can be expressed as

$$\mathbf{z}(t_{k+1}) = \mathbf{T}(t_{k+1}, t_k)\mathbf{z}(t_k), \quad k = 1, 2, \ldots, N, \quad (10)$$

where t_k and t_{k+1} refer to the start and end times of the kth period, with $t_1 = t$, $t_{N+1} = t + T_m$, and $t_{k+1} = t_k + \delta$. When N is sufficiently large that $\delta \ll T_m$, the modulated mass can be considered as constant in each portion. Under this condition, $\mathbf{T}(t_{k+1}, t_k)$ is time-independent over the period (t_k, t_{k+1}), and can be expressed as a Taylor series

$$\mathbf{T}(t_{k+1}, t_k) = \mathbf{T}(t_{k+1}, t_k) + \delta \frac{d\mathbf{T}(t_{k+1}, t_k)}{dt}\bigg|_{t_k}$$

$$+ \frac{\delta^2}{2!} \frac{d^2\mathbf{T}(t_{k+1}, t_k)}{dt^2}\bigg|_{t_k} + o(\delta^2). \quad (11)$$

We substitute Eq. (7) into Eq. (11) and ignore the high-order terms of δ, giving rise to

$$\mathbf{T}(t_{k+1}, t_k) = \mathbf{I} + \delta\mathbf{R}(t_k) + \frac{\delta^2}{2!}\left[\mathbf{R}^2(t_k) + \frac{d}{dt}\mathbf{R}(t_k)\right]. \quad (12)$$

From Eq. (12), the state transition matrix over one modulation period $\mathbf{T}(t + T_m, t)$ can be calculated from

$$\mathbf{T}(t + T_m, t) = \prod_{k=1}^{N} \mathbf{T}(t_{N-k+2}, t_{N-k+1}). \quad (13)$$

According to the Bloch theorem, the solution of this time-periodic-mass system satisfies [35]

$$\mathbf{z}(t + T_m) = e^{i\omega T_m}\mathbf{z}(t), \quad (14)$$

where ω is the complex eigenfrequency of a Floquet harmonic. By comparing Eqs. (9) and (14), we obtain

$$\mathbf{T}(t + T_m, t)\mathbf{z}(t) = \lambda\mathbf{z}(t), \quad \text{where } \lambda = e^{i2\pi\omega/\omega_m}. \quad (15)$$

Equation (15) describes a linear eigenproblem with an eigenvalue λ, and $\mathbf{z}(t)$ is the associated eigenvector. The eigenfrequency ω can be computed by solving the characteristic polynomial,

$$\det[\mathbf{T}(\omega_m) - \lambda(\omega/\omega_m)\mathbf{I}] = 0. \quad (16)$$

C. Harmonic balance method

An alternative method to solve the eigenvalue problem for the time-modulated system is based on the harmonic balance. According to this method, the eigenfrequency ω can be estimated by seeking a harmonic solution [41],

$$u(t) = a(t)e^{i\omega t}, \quad (17)$$

where $a(t)$ denotes the modulation amplitude of the displacement $u(t)$, and satisfies $a(t + T_m) = a(t)$. The amplitude $a(t)$ can be expressed as a Fourier series of the following form:

$$a(t) = \sum_{p=-\infty}^{\infty} a_p e^{ip\omega_m t}, \quad (18)$$

where a_p is the Fourier coefficient of the pth-order mode. The time-varying mass $M(t)$ can be expressed as

$$M(t) = \sum_{q=-\infty}^{\infty} M_q e^{iq\omega_m t}, \quad (19)$$

where M_q denotes the Fourier coefficient of order q and is given by

$$M_q = \frac{1}{T_m} \int_0^{T_m} M(t)e^{-iq\omega_m t}\, dt. \quad (20)$$

By substituting Eqs. (17)–(20) into Eq. (3) and performing the harmonic balance, the equations governing all pth-order modes can be derived as

$$\sum_{q=-\infty}^{\infty}\left[\left(\frac{\omega}{\omega_m}\right)^2 + (2p - q)\frac{\omega}{\omega_m} + p(p - q)\right]M_q a_{p-q}$$

$$- \frac{K}{\omega_m^2}a_p = 0, \quad p \in (-\infty, \infty). \quad (21)$$

We set a truncation order P for p, such that $a_p = 0$ for $|p| > P$. The range of q is given by $q \in [p - P, p + P]$.

Then Eq. (21) can be written in the form of a quadratic eigenvalue equation,

$$\left[\left(\frac{\omega}{\omega_m}\right)^2 \mathbf{L}_2 + \frac{\omega}{\omega_m}\mathbf{L}_1 + \mathbf{L}_0 - \left(\frac{\omega_0}{\omega_m}\right)^2 \mathbf{I} \right] \mathbf{a} = 0, \quad (22)$$

where $\omega_0 = \sqrt{K/M_0}$. $\mathbf{L}_0$, $\mathbf{L}_1$, and $\mathbf{L}_2$ are matrices of size $(2P+1) \times (2P+1)$, whose elements in the mth row and nth column are given by

$$\begin{aligned}
\mathbf{L}_0\,(m,n) &= (m-P-1)\,(n-P-1)\,M_{m-n}/M_0, \\
\mathbf{L}_1\,(m,n) &= (m+n-2P-2)\,M_{m-n}/M_0, \quad (23) \\
\mathbf{L}_2\,(m,n) &= M_{m-n}/M_0.
\end{aligned}$$

An equivalent form of Eq. (22) is given by

$$\begin{aligned}
&\begin{bmatrix} -\mathbf{L}_1 & -\mathbf{L}_0 + (\omega_0/\omega_m)^2\mathbf{I} \\ \mathbf{I} & 0 \end{bmatrix} \begin{bmatrix} (\omega/\omega_m)\mathbf{a} \\ \mathbf{a} \end{bmatrix} \\
&= \frac{\omega}{\omega_m} \begin{bmatrix} \mathbf{L}_2 & 0 \\ 0 & \mathbf{I} \end{bmatrix} \begin{bmatrix} (\omega/\omega_m)\mathbf{a} \\ \mathbf{a} \end{bmatrix}. \quad (24)
\end{aligned}$$

Consider the fact that the matrix $\mathbf{L_2}$ in Eq. (23) is real and symmetric. Equation (24) can, after some manipulation, be arranged in the form of a linear eigenvalue problem,

$$\mathbf{A}\mathbf{x} = \beta\mathbf{x}, \quad (25)$$

where the eigenvalue is $\beta = \omega/\omega_m$, with an eigenvector $\mathbf{x} = [\beta\mathbf{a}, \mathbf{a}]^T$. The matrix $\mathbf{A}$ is given by

$$\mathbf{A} = \begin{bmatrix} -\mathbf{L}_2^{-1}\mathbf{L}_1 & -\mathbf{L}_2^{-1}\left(\mathbf{L}_0 - (\omega_0^2/\omega_m^2)\mathbf{I}\right) \\ \mathbf{I} & 0 \end{bmatrix}. \quad (26)$$

The eigenvalue β can be calculated by solving the equation

$$\det\left[\mathbf{A} - \beta\mathbf{I}\right] = 0. \quad (27)$$

III. EXCEPTIONAL POINTS INDUCED BY TIME-VARYING MASS

A. Exceptional-point phenomenon

Consider the system parameters $\alpha = 0.2$ and $\omega_0 = 1$ rad/s. Figures 2(a) and 2(b) show the real and imaginary parts of the complex eigenfrequency ω/ω_0 plotted against the modulation frequency ω_m/ω_0, calculated using the state-space method with $N = 1000$. Equation (15) states that λ is a periodic function of $\mathrm{Re}(\omega)$ following $\lambda(\omega) = \lambda(\omega + n\omega_m)$, where n is an integer. Therefore, the complex values of ω have an infinite number of periodic solutions with a period of ω_m for the real part, and share the same imaginary part. Two distinct phases can be distinguished in the complex-eigenfrequency spectrum, characterized by bifurcations of the $\mathrm{Re}(\omega/\omega_0)$ and $\mathrm{Im}(\omega/\omega_0)$ curves, respectively. The splitting solutions for ω coalesce at specific values of $\omega_m/\omega_0 = 1.91$ and 2.12, which define phase transition points with the same signatures as those of EPs in non-Hermitian systems. To demonstrate the EP behavior at these two points, the coalescing of the eigenvectors needs to be analyzed. We denote the two sets of eigenstate solutions of Eq. (15) by $\{\lambda_1, \mathbf{z}_1\}$ and $\{\lambda_2, \mathbf{z}_2\}$, and construct a similarity transformation matrix $\mathbf{U}$ with eigenvectors in the form of $\mathbf{U} = [\mathbf{z}_1, \mathbf{z}_2]$. The determinant of $\mathbf{U}$ is never zero unless the two eigenvectors are degenerate. Thus, degeneracy of the eigenvectors, that is, $\mathbf{z}_1 = \mathbf{z}_2$,
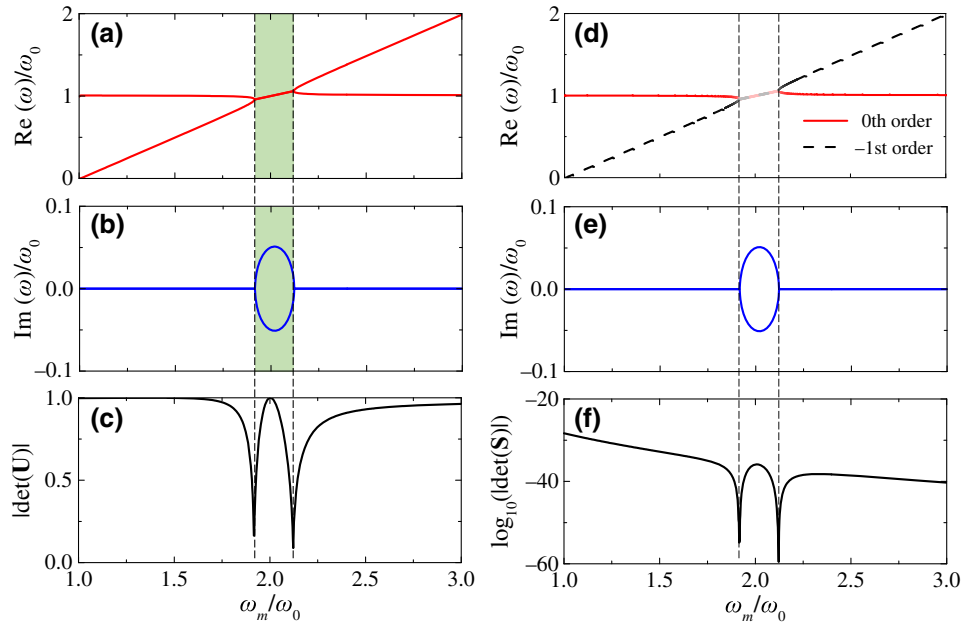

FIG. 2. (a) Real and (b) imaginary parts of complex eigenfrequency and (c) $|\det(\mathbf{U})|$ versus ω_m/ω_0, calculated by the state-space method. (d),(e) Complex eigenfrequency and (f) $\log_{10}(|\det(\mathbf{S})|)$ computed by the harmonic balance method.

can be identified by estimating whether or not the condition $|\det(\mathbf{U})| = 0$ is satisfied. Figure 2(c) plots the values of $|\det(\mathbf{U})|$ versus ω_m/ω_0, showing clearly a significant drop of $|\det(\mathbf{U})|$ at points with $\omega_m/\omega_0 = 1.91$ and 2.12. We have now demonstrated the occurrence of EPs induced by a time-varying mass. It is noted that the modulation frequency for the emergence of EPs can be changed when the system parameter α varies in the region $0 < \alpha < 1$.

Based on the state-space method, an analytic expression for the eigenfrequency ω for EPs to occur can be theoretically derived, as illustrated below. Let us revisit the eigenvalue problem described in Eq. (15). Because $\mathbf{T}(t + T_m, t)$ is a real 2×2 matrix, the two eigenvalues $\lambda_{1,2}$ must be either both real or a complex conjugate pair. To proceed, the eigenvalue λ defined in Eq. (15) is expressed in terms of complex eigenfrequencies $\omega = \omega' + i\omega''$ as

$$\lambda = e^{-2\pi\omega''/\omega_m}[\cos(2\pi\omega'/\omega_m) + i\sin(2\pi\omega'/\omega_m)], \quad (28)$$

where ω' and ω'' represent the real and imaginary parts, respectively, of ω. For the example studied in Fig. 2, it is verified through numerical calculations that $\det(\mathbf{T}(t + T_m, t)) = 1$ over the range of values of ω_m studied, which means that $\lambda_1\lambda_2 = 1$. While this equality is valid for the present example, its validity in the general case is still to be verified. We proceed with the discussion by analyzing the following two cases separately.

Case I. λ_1 and λ_2 are both real. We can obtain $\sin(2\pi\omega'_{1,2}/\omega_m) = 0$ from Eq. (28). This equation leads to the solutions $\omega'_{1,2} = n\omega_m/2$, such that $\lambda_{1,2} = \pm e^{-2\pi\omega''_{1,2}/\omega_m}$. From $\lambda_1\lambda_2 = e^{-2\pi(\omega''_1 + \omega''_2)/\omega_m} = 1$, we get $\omega''_1 + \omega''_2 = 0$. The eigenfrequencies are degenerate at EPs satisfying $\omega'_1 = \omega'_2$ and $\omega''_1 = \omega''_2$. If an EP exists, it occurs with an eigenfrequency ω satisfying $\omega'_1 = \omega'_2 = n\omega_m/2$ and $\omega''_1 = \omega''_2 = 0$.

Case II. λ_1 and λ_2 are a complex conjugate pair. We can obtain from Eq. (28) that $e^{i2\pi\omega'_1/\omega_m} = e^{-i2\pi\omega'_2/\omega_m}$ and $e^{-2\pi\omega''_1/\omega_m} = e^{-2\pi\omega''_2/\omega_m}$. These equations result in the relations $\omega'_1 + \omega'_2 = n\omega_m$ and $\omega''_1 = \omega''_2$, such that $\lambda_1\lambda_2 = e^{-4\pi\omega''_1/\omega_m}$. From $\lambda_1\lambda_2 = 1$, we have $\omega''_1 = \omega''_2 = 0$. If an EP exists, it appears with $\omega'_1 = \omega'_2 = n\omega_m/2$.

The analyses in the above two cases lead to the same conclusion, that EPs emerge at the eigenfrequency $\omega = n\omega_m/2$, which is in accordance with the result shown in Figs. 2(a) and 2(b).

Figures 2(d) and 2(e) plot the complex eigenfrequency ω/ω_0 computed using the harmonic balance method with a truncation order $P = 12$, and the results are in excellent agreement with Figs. 2(a) and 2(b). The coalescing of eigenvectors can be demonstrated in a similar manner to Fig. 2(c). There are $M = 4P + 2$ eigenvectors, denoted here by $\mathbf{x}_n$ ($n = 1, 2, \ldots, M$). The similarity transformation matrix $\mathbf{S}$ can be grouped as $\mathbf{S} = [\mathbf{x}_1, \ldots, \mathbf{x}_M]$. Figure 2(f) shows that $|\det(\mathbf{S})|$ is greatly lowered when

the modulation frequency approaches the phase transition point, validating our expectation of coalescence of the eigenvectors.

It is noteworthy that the harmonic balance method allows us to distinguish the contributions of different-order modes to the eigenfrequency spectrum. By substituting Eq. (18) into Eq. (17), we have $u(t) = \sum_{p=-\infty}^{\infty} a_p e^{i(\omega + p\omega_m)t}$. The branch for the pth-order mode has an eigenvector in which the component a_p is obviously large in magnitude compared with the others. Thereby, the contribution of the pth-order mode can be quantified by weighting the magnitude of a_p in the associated eigenvector $\mathbf{x}$. By using the above filtering method, the spectrum of $\mathrm{Re}(\omega)$ is found to be dominated by the fundamental mode ($p = 0$) and the first-order harmonics ($p = -1$), as presented in Fig. 2(d). It is clearly seen that the transition of the $\mathrm{Re}(\omega)$ spectrum from the bifurcation to the coalescing phase is caused by a coupling interaction between these two modes of different order.

B. Variation of eigenvalues with system perturbations near EPs

The EP phenomenon shown in Fig. 2 is caused by the coalescence of two eigenstates, and thus it is usually called a second-order EP. The salient property that the eigenvalue near an EP is highly sensitive to system perturbations is studied in this section. We denote the two eigenvalues relevant to the $p = 0, -1$ modes by β_1 and β_2 and assume that they coalesce at an EP with $\beta_{\mathrm{EP}} = \beta_{1,2}$. Using a similarity transformation matrix $\mathbf{S}$, the matrix $\mathbf{A}$ in Eq. (25) at an EP can be expressed in the Jordan normal form [13]

$$\mathbf{A}_{\mathrm{EP}} = \mathbf{S}\begin{bmatrix} \mathbf{J}(\beta_{\mathrm{EP}}) & \mathbf{0} \\ \mathbf{0} & \mathbf{W} \end{bmatrix}\mathbf{S}^{-1}, \quad (29)$$

where $\mathbf{J}(\beta_{\mathrm{EP}})$ is a 2×2 Jordan block given by

$$\mathbf{J}(\beta_{\mathrm{EP}}) = \begin{bmatrix} \beta_{\mathrm{EP}} & 1 \\ 0 & \beta_{\mathrm{EP}} \end{bmatrix}. \quad (30)$$

The matrix $\mathbf{W}$ denotes the Jordan normal form of the remaining parts of the eigenvalues. Next, let us introduce a perturbation ε into any of the system parameters relative to the EP position. The perturbed matrix is denoted by $\mathbf{A}'(\varepsilon)$, with $\mathbf{A}'(\varepsilon = 0) = \mathbf{A}_{\mathrm{EP}}$. We define the following characteristic polynomial pertaining to $\mathbf{A}'(\varepsilon)$ and β:

$$f(\varepsilon, \beta) = \det\left[\mathbf{A}'(\varepsilon) - \beta\mathbf{I}\right]. \quad (31)$$

By solving $f(\varepsilon, \beta) = 0$, which is equivalent to Eq. (27), the eigenvalue solutions for β as a function of the perturbation ε can be obtained. Explicit expressions for them can be derived using the holomorphic implicit function theorem and the inverse function theorem [42], as briefly described below.

There exists the relation $f(0, \beta_{1,2} = \beta_{\text{EP}}) = 0$ when the EP is of second order. Then, in the vicinity of the EP, the function $f(0, \beta)$ can be expressed as

$$f(0, \beta) = (\beta - \beta_{\text{EP}})^2(\cdots). \qquad (32)$$

Equation (32) leads to the following results:

$$\frac{\partial f(0, \beta)}{\partial \beta}\bigg|_{\beta = \beta_{\text{EP}}} = 0, \qquad \frac{\partial^2 f(0, \beta)}{\partial \beta^2}\bigg|_{\beta = \beta_{\text{EP}}} \neq 0. \qquad (33)$$

The EP studied here refers to a point degeneracy in the parameter space, which implies that

$$\frac{\partial f(\varepsilon, \beta_{\text{EP}})}{\partial \varepsilon}\bigg|_{\varepsilon = 0} \neq 0. \qquad (34)$$

We now expand $f(\varepsilon, \beta)$ in a power series about $\varepsilon = 0$ and $\beta = \beta_{\text{EP}}$ as

$$f(\varepsilon, \beta) = \frac{\partial f(\varepsilon, \beta_{\text{EP}})}{\partial \varepsilon}\bigg|_{\varepsilon = 0} \varepsilon$$
$$+ \frac{1}{2!} \frac{\partial^2 f(0, \beta)}{\partial \beta^2}\bigg|_{\beta = \beta_{\text{EP}}} (\beta - \beta_{\text{EP}})^2, \qquad (35)$$

where Eqs. (33) and (34) are used and higher-order terms are neglected.

An explicit expression for $\varepsilon(\beta)$ as a function of β can be obtained in the neighborhood of $\beta = \beta_{\text{EP}}$ by using the holomorphic implicit function theorem [42]. With help of Eqs. (32) and (33), it is found that

$$\varepsilon(\beta = \beta_{\text{EP}}) = 0, \qquad \frac{d\varepsilon(\beta)}{d\beta}\bigg|_{\beta = \beta_{\text{EP}}} = \frac{d\varepsilon}{df}\frac{df}{d\beta}\bigg|_{\beta = \beta_{\text{EP}}} = 0. \qquad (36)$$

We expand $\varepsilon(\beta)$ in a power series about $\beta = \beta_{\text{EP}}$ and make use of Eq. (36), giving rise to

$$\varepsilon(\beta) \approx \frac{1}{2} \frac{d^2\varepsilon(\beta)}{d\beta^2}\bigg|_{\beta = \beta_{\text{EP}}} (\beta - \beta_{\text{EP}})^2, \qquad (37)$$

where the higher-order terms are neglected. By substituting Eq. (37) into Eq. (35), the coefficient term in Eq. (37) is found as

$$\frac{1}{2} \frac{d^2\varepsilon(\beta)}{d\beta^2}\bigg|_{\beta = \beta_{\text{EP}}} = -\frac{\frac{1}{2}(\partial^2 f(0, \beta)/\partial \beta^2)|_{\beta = \beta_{\text{EP}}}}{(\partial f(\varepsilon, \beta_{\text{EP}})/\partial \varepsilon)|_{\varepsilon = 0}}. \qquad (38)$$

Note that the result of Eq. (38) is nonzero, as can be inferred from Eqs. (33) and (34). The relation in Eq. (37) means that $\varepsilon(\beta)$ varies proportionally to the square of a small variation of β. According to Eqs. (37) and (38), the function $\beta(\varepsilon)$ near $\varepsilon = 0$ can be expressed as

$$\beta(\varepsilon) \approx \beta_{\text{EP}} \pm \gamma \varepsilon^{1/2}, \qquad (39)$$

where the coefficient γ is given by

$$\gamma = \sqrt{-\frac{(\partial f(\varepsilon, \beta_{\text{EP}})/\partial \varepsilon)|_{\varepsilon = 0}}{\frac{1}{2}(\partial^2 f(0, \beta)/\partial \beta^2)|_{\beta = \beta_{\text{EP}}}}}. \qquad (40)$$

Equation (39) shows that for very small perturbations $\varepsilon \ll 1$, the eigenvalues $\beta(\varepsilon)$ vary proportionally to the square root of the perturbation ε in the vicinity of an EP. This is known as the square-root behavior of a second-order EP, and can be utilized to enhance the detection sensitivity for small perturbations, as will be further addressed in the next section.

IV. SENSOR MODEL WITH HIGH SENSITIVITY FOR DETECTING DEFECTS

A. Sensitive response to small perturbations near EPs

Consider the model parameters used in Fig. 2, but with a perturbed stiffness $K(1 + \varepsilon)$. When the stiffness is not perturbed ($\varepsilon = 0$), it is shown that the system exhibits EPs at modulation frequencies $\omega_m/\omega_0 = 1.91$ and 2.12 with an eigenfrequency $\omega = \omega_m/2$, denoted here by ω_{EP} for brevity. The complex eigenfrequencies ω/ω_m as a function of the perturbation ε in the two cases $\omega_m/\omega_0 = 1.91$ and 2.12 are shown in Figs. 3(a) and 3(b), respectively. The eigenfrequency ω is calculated from the exact eigenvalue problem and the approximate equation as described in Eq. (39), and excellent agreement between two results can be seen. When $\text{Re}(\omega)$ or $\text{Im}(\omega)$ splits into two branches, a small perturbation ε leads to a much larger change in the branch values due to the square-root behavior, and this property can be exploited to design highly sensitive sensors.

We proceed to analyze the forced-vibration response of the time-periodic-mass system to get further insights into the square-root behavior. A displacement excitation is applied to the end of the spring, with the form $U_0(t) = A \sin \omega_c t$, and the displacement response $u(t)$ of the mass element is governed by

$$\frac{1}{K(1 + \varepsilon)} \frac{d}{dt}\left[M(t)\frac{d}{dt}u(t)\right] + u(t) = U_0(t). \qquad (41)$$

The above equation is solved by a fourth-order Runge-Kutta method with zero initial displacement and velocity.

As an illustrative example, we lock the EP at a modulation frequency $\omega_m/\omega_0 = 2.12$ and choose $\omega_c = \omega_{\text{EP}}$ for the source excitation. The displacement response $u(t)/A$ in the time domain is shown in Figs. 4(a)–4(c) for $\varepsilon = 0$,
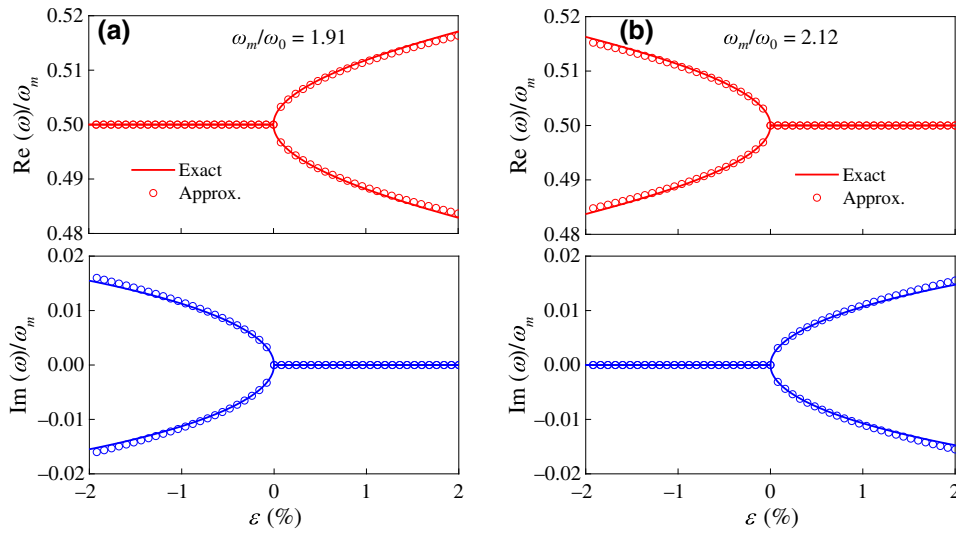
FIG. 3. Real and imaginary parts of complex eigenfrequency given by exact solutions of eigenvalue problem (solid line) and approximate solutions (open circles) calculated from Eq. (39) plotted against a small perturbation ε in two cases: (a) $\omega_m/\omega_0 = 1.91$; (b) $\omega_m/\omega_0 = 2.12$.

-0.01, and 0.01, respectively, and the respective frequency spectra are plotted in Figs. 4(d)–4(f).

In the absence of a perturbation ($\varepsilon = 0$), a sharp resonance peak appears at a frequency exactly equal to the eigenfrequency of the EP, namely $\omega = \omega_{\mathrm{EP}}$. By contrast, the response is characterized by two sharp peaks for $\varepsilon = -0.01$, and it is not difficult to verify that the peak

frequencies coincide with the splitting values of $\mathrm{Re}(\omega)$ as shown in Fig. 3(b). Notice that the sharp peak profile observed here is attributed to the zero imaginary part of the eigenfrequency ω for a negative ε. Now let us define a normalized splitting frequency for the double-peak response as $|\omega_1 - \omega_2|/\omega_{\mathrm{EP}}$, with $\omega_{1,2}$ denoting the two peak frequencies; this signifies the extent to which the two peaks
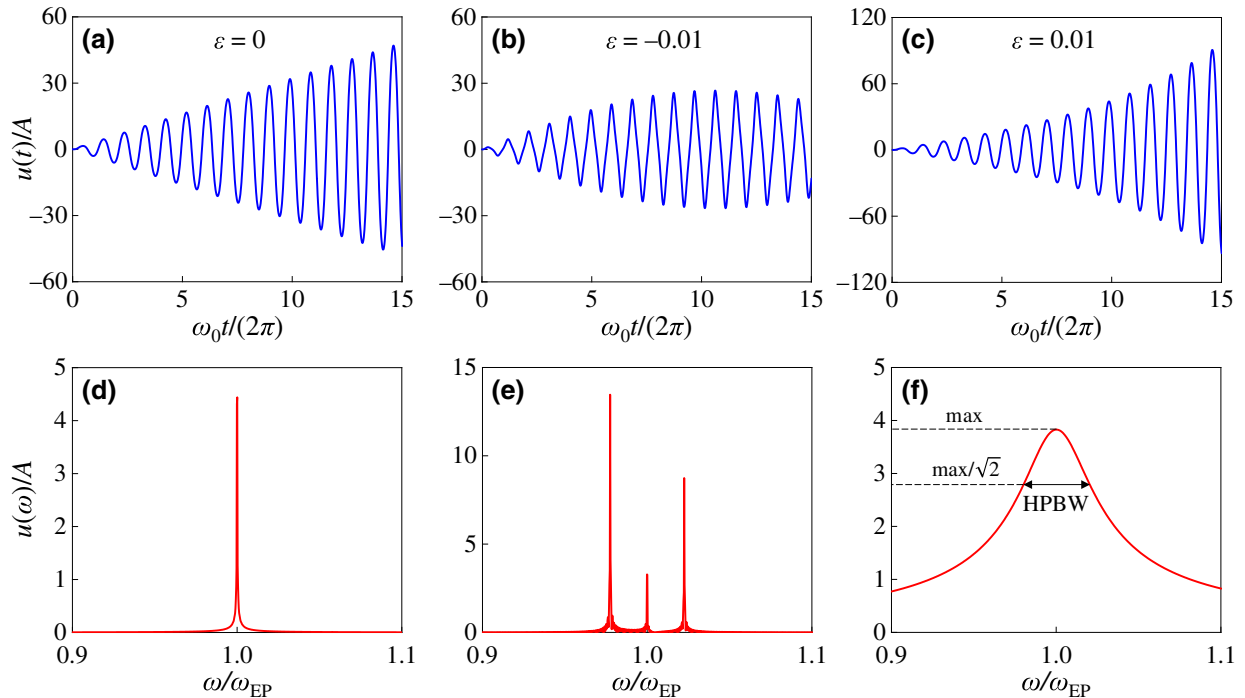

FIG. 4. Forced-vibration response of time-modulated system: (a)–(c) displacement response in the time domain for $\varepsilon = 0$, -0.01, and 0.01; (d)–(f) the respective frequency spectra. HPBW, half-power bandwidth.
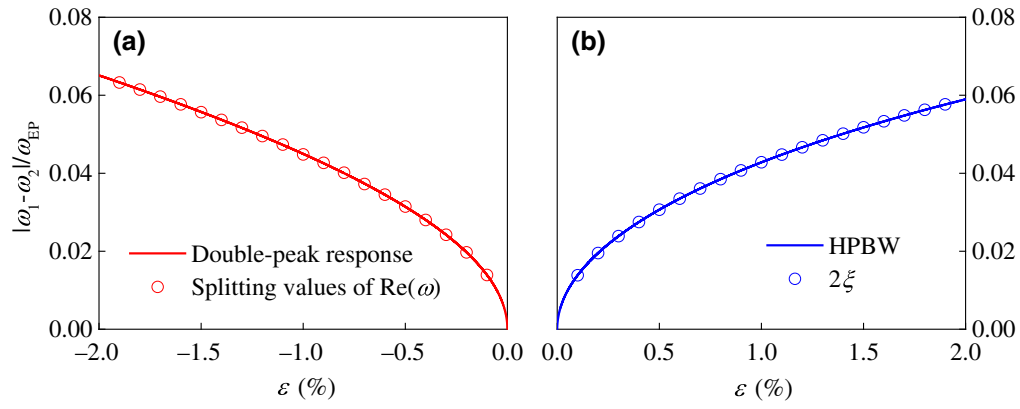
FIG. 5. (a) Normalized splitting frequency retrieved from the double-peak response and the splitting values of $\text{Re}(\omega)$ for negative-ε perturbations; (b) HPBW and damping factor 2ξ for positive-ε perturbations.

are separated. This quantity can also be used to evaluate the eigenfrequency, but with $\omega_{1,2}$ denoting the two splitting values of $\text{Re}(\omega)$. For various negative-ε perturbations, Fig. 5(a) plots the normalized splitting frequency retrieved from the double-peak response and the eigenfrequency solution for $\text{Re}(\omega)$, and the two results coincide very well. The frequency splitting of the resonance peak is governed by the square-root behavior, showing high-sensitivity performance with respect to a small perturbation. This is the critical concept behind the use of an EP in the design of ultrasensitive sensors.

For a positive-ε perturbation, the imaginary part of the eigenfrequency ω is nonzero, as seen in Fig. 3(b). This explains the flattening of the response curve for $\varepsilon = 0.01$ in Fig. 4(f). The bandwidth broadening can be characterized by the HPBW, which measures the bandwidth when the amplitude has dropped to $1/\sqrt{2}$ of its maximum value. On the other hand, an effective damping ratio $\xi = |\text{Im}(\omega)/\text{Re}(\omega)|$ can be defined from the eigenfrequency solutions, and this describes the time-decay effect in the form $e^{-\xi\,\text{Re}(\omega)t}$. We calculate the results for the HPBW and 2ξ for different negative-ε perturbations, as plotted in Fig. 5(b), and find good agreement between them. The result reflects a large variation of the HPBW for a small perturbation, which in turn causes a drastic change in the quality factor, which can be exploited in designing ultrasensitive sensors.

B. Sensor model with high sensitivity to void defects in elastic solids

Based on the square-root behavior near EPs, we postulate a sensor model that demonstrates enhanced sensitivity for detecting small void defects embedded within an elastic plate. The working mechanism of the sensor model is sketched in Fig. 6(a). The device comprises a time-varying-mass structure and a force sensor, which are placed on opposite sides of the plate to be tested. An excitation is applied to the backing side of the force sensor.

This structural model works in a similar way to the mass-spring model studied previously. The elastic solid behaves like a spring. An internal void defect acts as a small perturbation ε added to the spring stiffness and can be recognized from the splitting-frequency response of the force sensor. One can move the sensor device to detect void defects that may occur anywhere in the plate.

The performance of the sensor device is numerically investigated by use of a finite-element model, as shown in Fig. 6(b). To simplify the problem, the detection zone of the sensor is taken as a cylindrical body with diameter 2 cm and height 2 cm. The elastic solid has a Young's modulus of 6.11 MPa, a Poisson's ratio of 0.49, and a mass density of 670 kg/m^3. The time-varying mass $M(t)$ follows Eq. (1), with $M_0 = 10$ g and $\alpha = 0.2$. The displacement
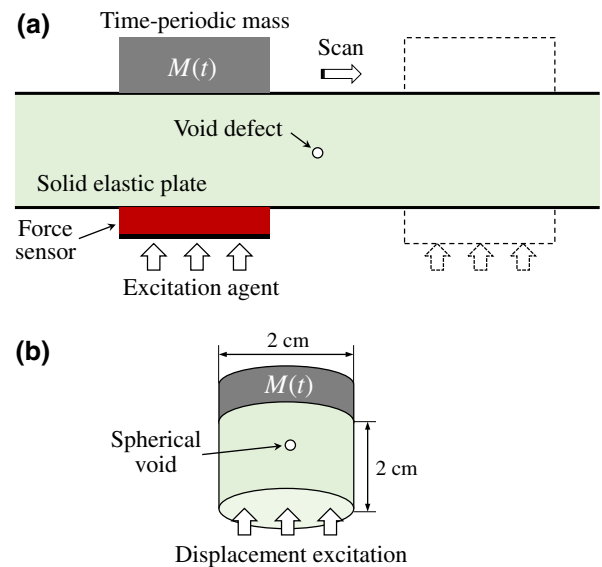

FIG. 6. (a) Working mechanism of an EP-based sensor to detect void defects. (b) Numerical-simulation model of the EP-based sensor.
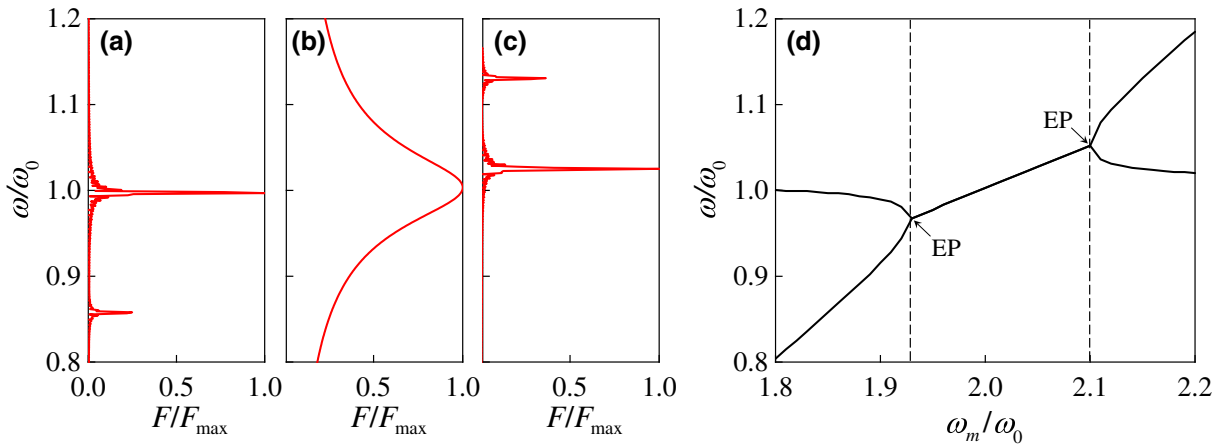
FIG. 7. (a)–(c) Frequency spectra of force signals for three typical cases, $\omega_m/\omega_0 = 1.85$, 2.0, and 2.15, respectively. (b) Peak response frequencies for different modulation frequencies.

excitation is applied to the bottom side of the elastic cylinder and has the same form as that used in Fig. 4. The time-domain force signals at the excitation surface are calculated and converted to a frequency-response spectrum by means of a Fourier transform. The numerical model is solved by the software package COMSOL Multiphysics.

To employ an EP for defect detection, the modulation frequency ω_m for an EP to occur needs to be identified first. According to the theoretical prediction shown in Fig. 2, EPs appear near $\omega_m = 2\omega_0$, where ω_0 here is the resonant frequency of a structural model with a constant mass M_0. By calculation of the response spectrum of the constant-mass model, a resonant frequency $\omega_0 = 3128$ rad/s is found. Numerical calculations are then conducted for the time-varying-mass model, with ω_m ranging from $1.8\omega_0$ to $2.2\omega_0$. Figures 7(a)–7(c) depict the frequency spectra of the force signals for the three typical cases $\omega_m/\omega_0 = 1.85$, 2.0, and 2.15 respectively, where the force spectrum is averaged over the excitation surface and normalized to its maximum value. Peak-response performance analogous to the results in Fig. 4 can be seen. We retrieve the peak response frequencies for various modulation frequencies, as plotted in Fig. 7(d). It is known that the EPs here correspond to bifurcation points in the parameter space of ω_m. Thus, the modulation frequencies for EPs to occur are found as $\omega_m/\omega_0 = 1.93$ and 2.10.

As a comparative model, we devise a resonance-shift (RS) sensor by letting $M(t) = M_0$. This sensor detects void defects by measuring the shift of the resonance frequency caused by softening of the stiffness due to voids. Figure 8(a) shows the frequency spectra of the force signals for the constant-mass model without and with a spherical void having a very small volume fraction of 0.5%. In the presence of this void defect, the normalized resonance frequency ω/ω_0 is shifted to 0.992, which implies a 0.8% change. The shift of the resonance frequency for different void volume fractions is calculated, as plotted in

Fig. 9, and a linear relationship between the two quantities is found. This shows the low-sensitivity nature of conventional RS sensors for detecting small perturbations. For an illustration of the enhanced sensitivity of the EP sensor, we choose the EP that occurs at $\omega_m/\omega_0 = 2.10$, with a peak response frequency $\omega_{EP} = 1.05\omega_0$. With the inclusion of a void defect with volume fraction 0.5%, the force frequency spectrum, as presented in Fig. 8(b), is characterized by two resonance peaks located at $\omega/\omega_{EP} = 0.973$ and 1.027, with a separation percentage of 5.4%, nearly 7 times larger than that for the RS sensor. We further calculate the split
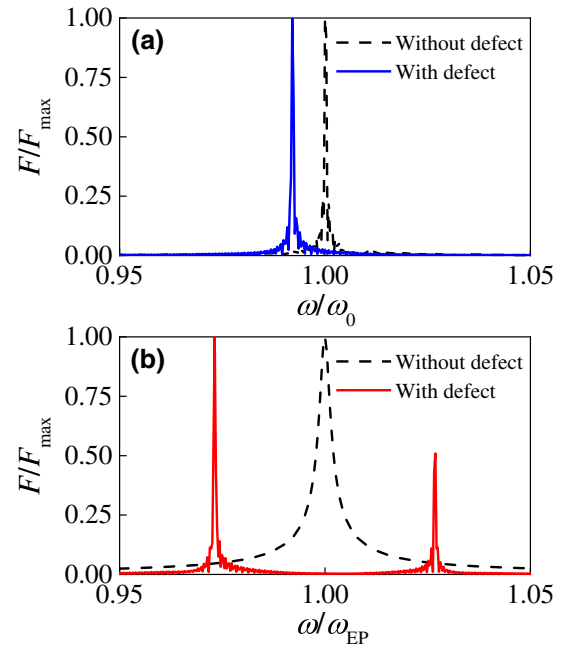

FIG. 8. Frequency spectra of force signals given by (a) RS sensor and (b) EP sensor for testing materials, with and without a void defect.
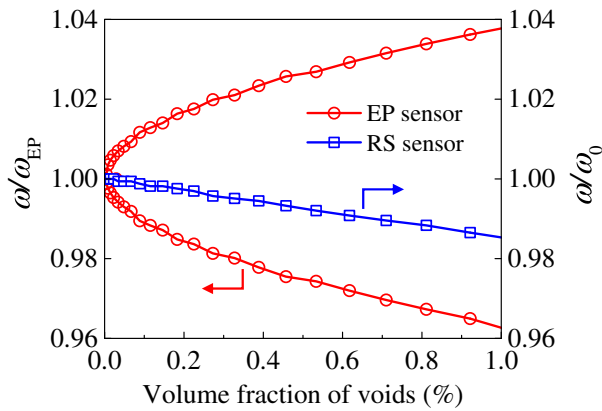
FIG. 9. Frequency shift of RS sensor and frequency splitting of EP sensor for testing materials with void defects with various volume fractions.

resonance frequencies for various void volume fractions, as shown in Fig. 9. The curve follows strictly a square-root behavior, explaining the EP-based mechanism for the sensitivity enhancement.

In the model studied, the modulation frequency serves as a control parameter that can be dynamically tuned to lock the EP position. We can also activate the other EP by choosing $\omega_m/\omega_0 = 1.93$, and then the sensor will be able to detect a stiff inclusion with enhanced sensitivity.

V. CONCLUSIONS

An exceptional point is usually created in multidegree-of-freedom systems, where two or more eigenvalues and eigenvectors coalesce simultaneously. In this paper, we report the construction of EPs in single resonators with a time-varying mass, which generate EPs by means of the coalescence of fundamental and harmonic eigenmodes. Based on the state-space and harmonic balance methods, a theoretical formulation of the eigenvalue problem for the time-modulated system is developed to demonstrate the existence of second-order EPs. We also show that the eigenvalues near EPs vary proportionally to the square root of a small perturbation. This unique feature is used to design an EP-based sensor model, which could enhance the sensitivity for detecting void defects in elastic plates. The proposed model may have potential applications in the development of high-sensitivity mechanical sensors.

[1] P. Hauptmann, Resonant sensors and applications, Sens. Actuators, A **26**, 371 (1991).

[2] G. Stemme, Resonant silicon sensors, J. Micromech. Microeng. **1**, 113 (1991).

[3] A. L. Herrera-May, L. A. Aguilera-Cortés, P. J. García-Ramírez, and E. Manjarrez, Resonant magnetic field sensors based on MEMS technology, Sensors **9**, 7785 (2009).

[4] L. Ren, M. Cong, and Y. Tan, An hourglass-shaped wireless and passive magnetoelastic sensor with an improved frequency sensitivity for remote strain measurements, Sensors **20**, 359 (2020).

[5] P. Fathi, J. Aliasgari, and N. C. Karmakar, Wireless rotation sensor using dual-layered twofold spiral resonator, IEEE Antennas Wirel. Propag. Lett. **21**, 789 (2022).

[6] M. Denoual, D. Robbes, S. Inoue, Y. Mita, J. Grand, H. Awala, and S. Mintova, Thermal resonant zeolite-based gas sensor, Sens. Actuators, B **245**, 179 (2017).

[7] L. Xu and X. Fu, A micro resonant gas sensor with adjustable natural frequency, IEEE Trans. Indus. Electron. **68**, 5337 (2021).

[8] K. Mistry, V. H. Nguyen, M. Arabi, K. H. Ibrahim, H. Asgarimoghaddam, M. Yavuz, D. Muñoz-Rojas, E. Abdel-Rahman, and K. P. Musselman, Highly sensitive self-actuated zinc oxide resonant microcantilever humidity sensor, Nano Lett. **22**, 3196 (2022).

[9] G. De Simoni, G. Signore, M. Agostini, F. Beltram, and V. Piazza, A surface-acoustic-wave-based cantilever biosensor, Biosens. Bioelectron. **68**, 570 (2015).

[10] L. Zhao, Y. Zhao, Y. Xia, Z. Li, J. Li, J. Zhang, J. Wang, X. Zhou, Y. Li, Y. Zhao, and Z. Jiang, A novel CMUT-based resonant biochemical sensor using electrospinning technology, IEEE Trans. Indus. Electron. **66**, 7356 (2019).

[11] G. Nunzi Conti, S. Berneschi, and S. Soria, Aptasensors based on whispering gallery mode resonators, Biosensors **6**, 28 (2016).

[12] V. Pachkawade, State-of-the-art in mode-localized MEMS coupled resonant sensors: A comprehensive review, IEEE Sens. J. **21**, 8751 (2021).

[13] T. Kato, *Perturbation Theory for Linear Operators* (Springer, Berlin, Heidelberg, 1966), p. XXI, 623.

[14] M.-A. Miri and A. Alù, Exceptional points in optics and photonics, Science **363**, eaar7709 (2019).

[15] A. Welters, On explicit recursive formulas in the spectral perturbation analysis of a Jordan block, SIAM J. Matrix Anal. Appl. **32**, 1 (2011).

[16] W. Chen, Ş. Kaya Özdemir, G. Zhao, J. Wiersig, and L. Yang, Exceptional points enhance sensing in an optical microcavity, Nature **548**, 192 (2017).

[17] M. P. Hokmabadi, A. Schumer, D. N. Christodoulides, and M. Khajavikhan, Non-Hermitian ring laser gyroscopes with enhanced Sagnac sensitivity, Nature **576**, 70 (2019).

[18] T. Xing, Z. Pan, Y. Tao, G. Xing, R. Wang, W. Liu, E. Xing, J. Rong, J. Tang, and J. Liu, Ultrahigh sensitivity stress sensing method near the exceptional point of parity-time symmetric systems, J. Phys. D: Appl. Phys. **53**, 205102 (2020).

[19] Z. Dong, Z. Li, F. Yang, C.-W. Qiu, and J. S. Ho, Sensitive readout of implantable microsensors using a wireless system locked to an exceptional point, Nat. Electron. **2**, 335 (2019).

[20] Z. Xiao, H. Li, T. Kottos, and A. Alù, Enhanced Sensing and Nondegraded Thermal Noise Performance Based on PT-Symmetric Electronic Circuits with a Sixth-Order Exceptional Point, Phys. Rev. Lett. **123,** 213901 (2019).

[21] K. Ding, G. Ma, M. Xiao, Z. Q. Zhang, and C. T. Chan, Emergence, Coalescence, and Topological Properties of Multiple Exceptional Points and Their Experimental Realization, Phys. Rev. X **6,** 021007 (2016).

[22] K. Ding, G. Ma, Z. Q. Zhang, and C. T. Chan, Experimental Demonstration of an Anisotropic Exceptional Point, Phys. Rev. Lett. **121,** 085702 (2018).

[23] Y. Liu, Z. Liang, J. Zhu, L. Xia, O. Mondain-Monval, T. Brunet, A. Alù, and J. Li, Willis Metamaterial on a Structured Beam, Phys. Rev. X **9,** 011040 (2019).

[24] B. Lustig, G. Elbaz, A. Muhafra, and G. Shmuel, Anomalous energy transport in laminates with exceptional points, J. Mech. Phys. Solids **133,** 103719 (2019).

[25] V. Domínguez-Rocha, R. Thevamaran, F. Ellis, and T. Kottos, Environmentally Induced Exceptional Points in Elastodynamics, Phys. Rev. Appl. **13,** 014060 (2020).

[26] A. A. Mokhtari, Y. Lu, Q. Zhou, A. V. Amirkhizi, and A. Srivastava, Scattering of in-plane elastic waves at metamaterial interfaces, Int. J. Eng. Sci. **150,** 103278 (2020).

[27] G. Shmuel and N. Moiseyev, Linking Scalar Elastodynamics and Non-Hermitian Quantum Mechanics, Phys. Rev. Appl. **13,** 024074 (2020).

[28] Z. Gu, H. Gao, P.-C. Cao, T. Liu, X.-F. Zhu, and J. Zhu, Controlling Sound in Non-Hermitian Acoustic Systems, Phys. Rev. Appl. **16,** 057001 (2021).

[29] C. M. Bender and S. Boettcher, Real Spectra in Non-Hermitian Hamiltonians Having PT Symmetry, Phys. Rev. Lett. **80,** 5243 (1998).

[30] R. El-Ganainy, K. G. Makris, M. Khajavikhan, Z. H. Musslimani, S. Rotter, and D. N. Christodoulides, Non-Hermitian physics and PT symmetry, Nat. Phys. **14,** 11 (2018).

[31] J. Christensen, M. Willatzen, V. R. Velasco, and M.-H. Lu, Parity-Time Synthetic Phononic Media, Phys. Rev. Lett. **116,** 207601 (2016).

[32] Z. Hou and B. Assouar, Tunable elastic parity-time symmetric structure based on the shunted piezoelectric materials, J. Appl. Phys. **123,** 085101 (2018).

[33] Q. Wu, Y. Chen, and G. Huang, Asymmetric scattering of flexural waves in a parity-time symmetric metamaterial beam, J. Acoust. Soc. Am. **146,** 850 (2019).

[34] M. I. Rosa, M. Mazzotti, and M. Ruzzene, Exceptional points and enhanced sensitivity in PT-symmetric continuous elastic media, J. Mech. Phys. Solids **149,** 104325 (2021).

[35] H. Kazemi, M. Y. Nada, T. Mealy, A. F. Abdelshafy, and F. Capolino, Exceptional Points of Degeneracy Induced by Linear Time-Periodic Variation, Phys. Rev. Appl. **11,** 014007 (2019).

[36] J. Huang and X. Zhou, A time-varying mass metamaterial for non-reciprocal wave propagation, Int. J. Solids Struct. **164,** 25 (2019).

[37] M. S. Allen, Frequency-domain identification of linear time-periodic systems using LTI techniques, J. Comput. Nonlinear Dyn. **4,** 041004 (2009).

[38] R. W. Brockett, *Finite Dimensional Linear Systems* (Society for Industrial and Applied Mathematics, Philadelphia, PA, 2015), p. 67.

[39] G. Peano, Intégration par séries des équations différentielles linéaires, Math. Ann. **32,** 450 (1888).

[40] H. F. Baker, Note on the interation of linear differential equations, Proc. London Math. Soc. **s2-2,** 293 (1905).

[41] J. Vila, R. K. Pal, M. Ruzzene, and G. Trainiti, A Bloch-based procedure for dispersion analysis of lattices with periodic time-varying properties, J. Sound Vib. **406,** 363 (2017).

[42] S. G. Krantz, Function theory of several complex variables (American Mathematical Society, 1982), Chap. 1, p. 35.